Charge Mobility and Dynamics in Spin-Crossover Nanoparticles Studied by Time-Resolved Microwave Conductivity

Dugay, Julien; Evers, Wiel; Torres-Cavanillas, Ramón; Giménez-Marqués, Mónica; Coronado, Eugenio; Van Der Zant, Herre S.J.

DOI
10.1021/acs.jpclett.8b02267

Publication date
2018

Document Version
Final published version

Published in
Journal of Physical Chemistry Letters

THE JOURNAL OF PHYSICAL CHEMISTRY Letters

Letter

Cite This: J. Phys. Chem. Lett. 2018, 9, 5672−5678

pubs.acs.org/JPCL

Charge Mobility and Dynamics in Spin-Crossover Nanoparticles Studied by Time-Resolved Microwave Conductivity

Julien Dugay,*[,†,‡] Wiel Evers,[†,§] Ramón Torres-Cavanillas,[‡] Mónica Giménez-Marqués,[‡] Eugenio Coronado,*[,‡] and Herre S. J. Van der Zant[†]

[†]Kavli Institute of Nanoscience, Delft University of Technology, Lorentzweg 1, 2628 CJ Delft, The Netherlands

[‡]Instituto de Ciencia Molecular (ICMol), Universidad de Valencia, Catedrático José Beltrán 2, 46980 Paterna, Spain

[§]Optoelectronic Materials Section, Delft ChemTech, Faculty of Applied Sciences, Delft University of Technology, Julianalaan 136, 2628 BL Delft, The Netherlands

Supporting Information

ABSTRACT: We use the electrodeless time-resolved microwave conductivity (TRMC) technique to characterize spin-crossover (SCO) nanoparticles. We show that TRMC is a simple and accurate means for simultaneously assessing the magnetic state of SCO compounds and charge transport information on the nanometer length scale. In the low-spin state from liquid nitrogen temperature up to 360 K the TRMC measurements present two well-defined regimes in the mobility and in the half-life times, in which the former transition temperature T_R occurs near 225 K. Below T_R, we propose that an activationless regime taking place associated with short lifetimes of the charge carriers points at the presence of shallow-trap states. Above T_R, these states are thermally released, yielding a thermally activated hopping regime where longer hops increase the mobility and, concomitantly, the barrier energy. The activation energy could originate not only from intricate contributions such as polaronic self-localizations but also from dynamic disorder due to phonons and/or thermal fluctuations of SCO moieties.

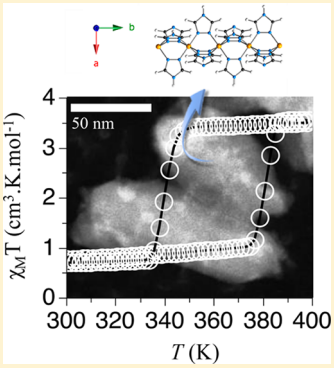

Spin-crossover (SCO) materials form a remarkable class of compounds with the ability to reversibly change their ground spin state between a low spin (LS) and a high spin (HS), triggered by a rich palette of external stimuli.[1−4] Temperature is the most common stimulus used to promote the entropy-driven population of the HS state at elevated temperatures, subverting the physical properties of the SCO materials such as a change in their magnetic moment, structure, and color. Moreover, first-order phase transitions arise when elastic interactions within dense arrays of SCO molecules overcome a certain threshold. When even stronger elastic interactions take place, thermal hysteresis loops may appear spanning room temperature. This feature may be of interest[2,3] for developing future technological applications.[1,5] In particular, nanoparticles (NPs) as small as 4 nm based on the Fe(II) triazole−triazolate polymeric chain complex with formula $[Fe(Htrz)_2(trz)](BF_4)$ (Htrz = 1,2,4-triazole and trz = triazolate) show abrupt transitions above room temperature, maintaining wide thermal memory effects of ca. 25 K.[6] Moreover, it has been previously shown that the amount of light reflected as a function of temperature is a simple and accurate means to assess the magnetic state of the studied SCO compounds.[7,8] Furthermore, these memory effects have been probed by electrical conductivity measurements both in powdered samples[9−11] and in micro-[12−15] and nanostructures[16−18] down to the single NP level.[19]

When the NP is incorporated into electronic devices, the conduction of the NP increases or decreases upon changing the ground spin state. From the LS to HS state, some of us showed that single NP devices exhibit an increase of the conductance,[19] while the reverse situation occurs for small assembles of similar SCO NPs.[17] A consistent decrease of the conductance in the HS state has also been demonstrated by the Bousseksou's group while investigating larger assemblies of ca. 15 nm sized NPs[20] and microrods[14,15,20−22] as well as powdered-samples of the same compound.[9,11] At this stage, it is tempting to attribute these opposite behaviors to separate charge transport regimes: (i) single-electron tunnelling transport within a double barrier tunnelling configuration for single NPs, when the gap size of the electrodes is of ca. 5−10 nm, as evidenced by a Coulomb staircase in the current−voltage characteristics at 10 K and the absence of thermal activation of the conductance above room temperature[19] and (ii) hopping transport for NP assemblies placed on gap sizes ranging from ca. 50 nm[17] up to several microns.[9,11,14,15,20−22] For larger SCO objects and electrode separation, a charge transport dominated by polaron hopping was proposed by Bousseksou's group, on the basis of the thermally activated conductivity above room temperature combined with rather small conductivity values.[9]

Received: July 22, 2018
Accepted: September 13, 2018
Published: September 13, 2018

DOI: 10.1021/acs.jpclett.8b02267
J. Phys. Chem. Lett. 2018, 9, 5672−5678

In the previous studies, charge carriers were generated via source-drain electrodes in direct contact with the SCO compounds. The influence of the electrodes and/or interparticle transport can be significantly reduced using AC electric fields as it confines the motion of the charge carriers into a smaller spatial area. Recently, thermal hysteresis loops in compacted powder samples of SCO microrods have been measured not only by broadband (10^{-2} to 10^{6} Hz) ac conductivity experiments but also from the dielectric losses and relaxation dynamics of the charge carriers.[11,22] However, the single-electron tunnelling to hopping transition aforementioned could not be proved in these cases, which requires higher frequencies: ac transport measurements should then be carried out at a greater electric field frequency to reach a charge displacement in the nanometre range.

Time-resolved microwave conductivity (TRMC) is a powerful method to quantify charge carrier mobilities and dynamics for various systems such as organic and inorganic semiconducting materials and photoactive molecular layers.[23,24] TRMC measurements do not employ ohmic contacts, thereby eliminating perturbations related to grain boundaries, dielectric polarization effects, space-charge effects, contact resistances, differences in the NP coupling, and charge injection at electrodes.

In this work, we report on the first TRMC study applied to SCO compounds. The mobilities of both electrons and holes as well as their relaxation kinetics have been monitored by measuring the absorbed power of a 9 GHz microwave field as a function of time.

Our investigations are focused on 100 nm size hybrid core−shell SCO@SiO_2 NPs, where the SCO corresponds to the Fe^{II}−triazole coordination polymer $[Fe(Htrz)_2(trz)](BF_4)$.[25,26] The crystal structure is based on polymeric chains of Fe^{II} ions with the three bridging triazoles, two Htrz ligands and one trz^- ligand and charge balanced with a BF_4^- anion.[27,28] This compound presents an abrupt transition above room temperature with a stable hysteresis of ca. 40 K. The hybrid $[Fe(Htrz)_2(trz)](BF_4)$@SiO_2 system stabilized by an inorganic shell of silica (see supporting material for more details) was selected in view of its enhanced chemical robustness when submitted to thermal cycles in the range 300−400 K with the aim of measuring its hysteretic behavior.[18] Indeed, we have made unfruitful attempts with more conventional noncoated NPs in both a powder form and 2D assemblies on quartz slides. These NPs were stabilized in solution by AOT organic surfactants that quickly suffered temperature changes and avoided to draw any conclusions.

Characterization of the SCO@SiO_2 NPs. *Magnetic Properties.* The temperature-dependent magnetic susceptibility data of a powder sample of SCO@SiO_2 NPs is presented in Figure 1. Magnetic data were collected using a SQUID magnetometer and correspond to the second temperature cycle performed with heating and cooling constant sweep rates of 1 K min^{-1} under a magnetic field of 0.1 T. The spin transition features, regarding the value in the HS state of ∼3.5 cm^3 K mol^{-1}, the steepness of ∼10 K and the 40 K-wide thermal hysteresis loop, are consistent to that of the previous reported on similar systems.[29]

Composition. A representative high-angle annular dark-field scanning transmission electron microscopy HAADF-STEM image of the SCO@SiO_2 NPs is shown in the inset of Figure 1 (see also Figure S1). These NPs exhibit a rodlike shape with an average length of 109 ± 24 nm and a diameter of 45 ± 30 nm;

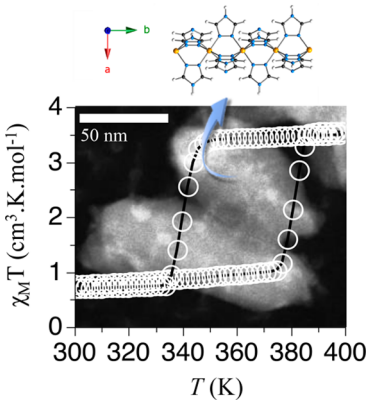

Figure 1. Magnetic thermal hysteresis loop of a powder sample of hybrid SCO NPs. A view of the cationic chains of $[Fe(Htrz)_2(trz)](BF_4)$ are displayed in which Fe^{II} are aligned parallel along the *b* axis with the three bridging triazoles in alternating invert positions (BF_4^- anions are omitted for clarity). This system exhibits a wide and abrupt hysteresis loop above room temperature. Inset: a representative TEM image acquired in STEM-HAADF mode of these NPs. The highly scattering areas appear as bright regions.

energy-dispersive X-ray (EDX) experiments confirmed the presence of an outer pure silica shell surrounding the NP cores as shown in Figure S2, Supporting Information.

Optical Properties. The total fraction of light absorbed (F_A) by a powder sample of SCO NPs compared to that for a highly reflecting reference sample at a fixed wavelength was estimated following eq 1:

$$F_A = 1 - (F_R + F_T) \quad (1)$$

where F_T, the incident laser light fraction transmitted through the powder sample, is equal to zero (see Figure S4). Optical diffuse reflectance (F_R) from powder samples of SCO@SiO_2 NPs have been acquired using a CARY 5G UV−vis−NIR spectrophotometer adapted with an integrating sphere, in the wavelength range 300−800 nm. The SCO core of the NPs exhibited well-known features of Iron(II) SCO complexes, that is to say, the absorption band in the visible centered at 530 nm (see Figure S5). Accordingly, this absorption band corresponds to one of the two spin-allowed ligand-field transitions $^1A_1$−$^1T_1$ in the LS state. The value of F_A was extracted in the low-spin state from the absorption spectra at 530 nm (F_A = 69%). These values have been exploited to quantitatively estimate the mobilities of SCO NPs measured via TRMC (see eq 2).

Time-Resolved Microwave Conductance (TRMC) Measurements. TRMC is a contactless technique that utilizes high-frequency microwaves to probe the conductivity increase induced by a laser pulse, an electron beam or X-rays. In this work, the charge carriers are photogenerated using an accordable laser and the transport properties are probed using 9 GHz microwaves (for more details see Supporting Information and Figure S6). The high-frequency microwave signal is provided by a peak amplitude of ca. 100 V/cm, which is low enough to prevent alteration of the compound itself and charge diffusion after their photogeneration. TRMC techniques offer a local probing scale typically close to the polymer chain or intermolecular distance.[24,23]

Effect of Dose in the Pulse on Charge Carrier Mobility. A quartz sample holder was specially designed to perform the time-resolved microwave conductivity measurements of powder samples of SCO@SiO_2 NPs (see an optical

DOI: 10.1021/acs.jpclett.8b02267
J. Phys. Chem. Lett. 2018, 9, 5672−5678

image taken at 300 K in Figure 2 and versus temperature in Movie S1). As the width of the quartz holder is thinner than

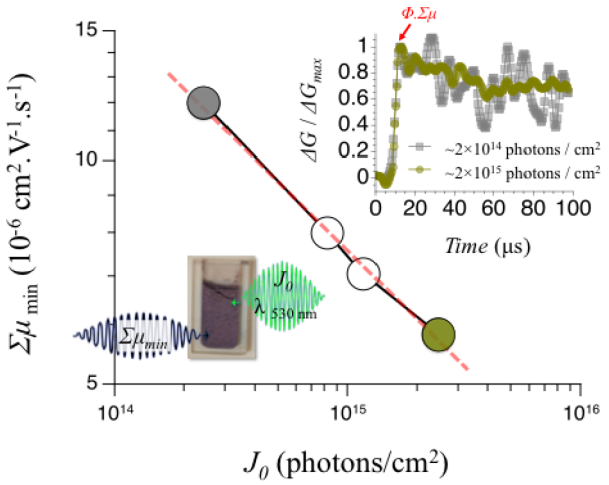

Figure 2. Maximum observed TRMC signals measured at room temperature as a function of incident photons per laser pulse J_0 excited at λ = 530 nm. The inset shows two TRMC signals (corresponding to the gray and yellow circles), normalized to the peak signal for clarity.

the powder thickness used for reflectance measurements, we ensured that F_T remained close to zero when the SCO NP powder was present in the quartz holder using diode laser excitation at 530 nm and a spectrophotometer in the wavelength range 300−900 nm (see Figure S4, Supporting Information).

Figure 2 presents the maximum TRMC signal change as a function of incident photon density per laser pulse, J_0. The latter was varied at room temperature using metallic neutral density filters. The photon wavelength was chosen to fall close to the peak of the LS state absorption band of the SCO NPs, i.e., λ = 530 nm. The TRMC signal is expressed as the product of the optical charge carrier generation quantum yield, ϕ, and the sum of electron and hole mobility, $\Sigma\mu$. This product is calculated according to[24]

$$\phi\Sigma\mu = \frac{\Delta G_{max}}{\beta e I_0 F_A} \quad (2)$$

where ΔG_{max} is the maximum measured change in conductance, β is the ratio between the quartz holder height and width perpendicular to the microwave vector, e is the elementary charge, I_0 is the number of photons per unit area per pulse, and F_A is the fraction of absorbed light.

The maximum conductivity change $\phi\Sigma\mu$, as pointed out by the red arrow in inset of this figure, was extracted from 1000 averaged transients after laser-pulse excitation. As TRMC signals remain rather low for such NP systems, we systematically subtracted from the dark conductance of the sample to avoid spurious responses. The net yield of mobile charge carriers per absorbed photon ϕ is not known for SCO compounds; however, it has to be smaller than or equal to 1. At short time scales after the pulse, ϕ is assumed to be close to unity, i.e., $\phi = \phi_{max} = 1$.[30] The product $\phi_{max}\Sigma\mu$ corresponds therefore either to a good approximation of the genuine electrical mobility of the charge carrier values or to a lower limit, referred after to as $\Sigma\mu_{min}$. The validity of the mobility estimate assumes that the optical quantum yield remains close to 1 for the studied range of optical fluence (while one can expect actually an optical quantum yield decrease with increasing optical fluence). In this scenario, a charge carrier mobility of ~1.2 × 10^{-5} cm^{-2}/(V s) is obtained at 2.4 × 10^{14} photons/cm^2 per pulse, which is the lowest intensity that still showed a sufficient signal-to-noise ratio. However, we observed a smaller mobility value of ~5.8 × 10^{-6} cm^{-2}/(V s) for 2.45 × 10^{15} photons/cm^2 per pulse, which is the highest intensity delivered by the TRMC setup.

The behavior of the maximum conductivity against the incident intensity is commonly described via a power law ($\Sigma\mu_{min} \propto J_0^{\delta}$).[31] In the case where only first-order decay processes take place (i.e., δ = 1), higher-order recombination occurs within the nanosecond laser when δ < 1. In Figure 2, δ equals 0.34 as deduced from the linear fit (red dashed line), suggesting that higher-order processes indeed occur at room temperature, at least for a decade of intensity change.[32] For all the next experiments, we fixed the laser intensity to the highest value of 2.45 × 10^{15} photons/cm^2 per pulse offering the best signal-to-noise ratio.

High-Temperature Dependence of the Charge Carrier Mobility Using TRMC. Figure 3 presents the

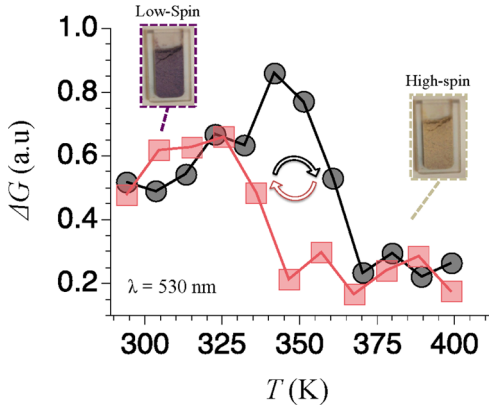

Figure 3. Normalized TRMC signals against temperature from room temperature up to 400 K. Optical photographs of the measured powder sample compacted in a quartz holder are shown on the left and right in the LS and HS states, respectively. The signal drop coresponds to an expected decrease of absorbance at λ = 530 nm, to which the TRMC technique is sensitive.

extracted maximum values of the conductivity transients for temperatures in the range 300 < T < 400 K. Representative microwave conductivity transients as a function of time in the heating and cooling modes at an elevated temperature of 350 K are shown in Figure S7, Supporting Information. Each transient was recorded after several tens of minutes to ensure thermal equilibrium and averaged over 1000 laser pulses. A clear difference in the change of conductance values can be observed depending on the thermal history of the sample depicting a 25 K thermal hysteresis loop. We stress that this hysteresis effect was reproducible over several weeks and that an empty quartz sample holder did not show such a temperature dependence as can be seen in Figure S7. Moreover, after all the TRMC measurements were taken, the same powder sample exhibited a well-known thermochromic effect above room temperature from purple to white/yellow, triggered by means of a hot plate (see also Movie S1). Hence, we can ascribe the hysteresis loop in the change of conductance to the associated first-order spin transition of

DOI: 10.1021/acs.jpclett.8b02267
J. Phys. Chem. Lett. 2018, 9, 5672−5678

these hybrid SCO@SiO_2 NPs. The origin of the thermal hysteresis loop in the change in conductance can be understood through the thermal reflectivity change of our SCO compounds, to which the TRMC technique is very sensitive. The amount of light reflected as a function of temperature has previously been proved to be a simple and accurate mean to assess the magnetic state of the studied SCO compounds.[7,8] An advantage given by the TRMC in this work is the ability to simultaneously obtain the thermal hysteresis loop features of SCO NPs and quantitative values of mobilities and dynamics of the charge carriers for different powder samples.

Mobility values in the LS state are in the range of $\sim 1 \times 10^{-(6\ \text{to}\ 5)}$ $cm^2\ V^{-1}\ s^{-1}$, in good agreement with the experimental value reported for a comparable SCO compound based on Fe(II). For instance, thin films of $Fe(phen)_2(NCS)_2$ showed a hole mobility of 6.53×10^{-6} $cm^2\ V^{-1}\ s^{-1}$ at room temperature (extracted from space charge-limited regime).[33] Nevertheless, the nature of the charge carriers remains unknown for the triazole-based SCO NPs as both electrons and holes can contribute to the observed photoconductivity using TRMC. It is also worthwhile to note that the extracted mobilities stand for the ensemble of NPs, which is isotropic as they are randomly oriented. Therefore, if it turns out that the transport is 1D, which is not yet proved for this SCO compound, the mobility that we measured in this work should be multiplied by a factor of 3.[34]

In an attempt to quantitatively compare the transport properties of the LS state with those in HS state, we photogenerated charge carriers at a longer wavelength centered at λ = 830 nm corresponding to HS optical absorption band maximum. As shown in Figure S9, the thermal dependence of the charge carrier mobility showed a thermal hysteresis loop similar to that observed while exciting the laser at 530 nm. However, the hysteresis loop is expected to be inversed in this case as the amount of photogenerated carriers should increase upon the thermally induced LS−HS transition at λ = 830 nm.[35] This observation leads to the conjecture that the dominant TRMC signal comes from the LS absorption band tail remaining at 830 nm (where F_A is of about 24%, see the Figure S5) rather than from the corresponding maximum of the HS absorption band. Consequently, we could not quantitatively compare the mobilities in both spin states.

Temperature Dependence of the Charge Carrier Mobility from 77 K up to 360 K. To get more insight into the charge transport mechanism in the LS state, we extended the TRMC measurements from liquid nitrogen temperature up to 360 K. Figure 4 presents the natural logarithm values of the maximum TRMC signal against inverse temperature. In these experiments, only a single wavelength was used for mobility estimations; thus wavelength calibration errors of the power meter can be neglected. Laser fluctuations can be ruled out as well, considering the long integration times of the measurements (several minutes for averaging each acquisition 1000 times) and the reliable stability of our laser thanks to stable experiment conditions (weak vibrations, stable temperature). Therefore, only a gradual drift of conductance change is expected going beyond the measurement acquisition time. For these reasons, we estimated that the error on mobility measurements is chiefly originating from read out noise thus being the error in determining the maximum conductance change signal. A strong monotonic decrease of the mobility with temperature is found. Furthermore, two

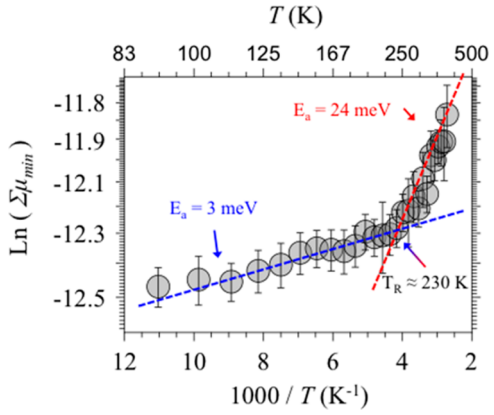

Figure 4. Natural logarithm of the maximum TRMC signal after laser pulse exciting at 530 nm versus reciprocal temperature. Two activation energies are deduced from an Arrhenius fit as presented by the dashed lines.

different regimes are found above and below a transition temperature of ca. 230 K. We extract the activation energies (E_a) using the following equation, above and below T_R, respectively:

$$\sum \mu_{\text{min}} \propto \exp\left(-\frac{\text{Ea}}{k_B T}\right) \tag{3}$$

The high-temperature range for $T > T_R$ exhibits thermal activation with a small activation energy of E_a = 24 ± 2 meV. In contrast, the mobility at the lower-temperature range, for $T < T_R$ can be viewed as activationles. Indeed, the extracted activation energy of 2.9 ± 0.2 meV corresponding to ca. 34 K remains lower than the temperature at which it was measured. Similar activation energy values were obtained upon reheating this sample to room temperature. Importantly, the temperature dependence of the empty quartz holder is distinctly different (see Figure S10, Supporting Information).

It is interesting to note that the activation energy of 24 meV extracted near room temperature is more than 1 order of magnitude lower than that reported in the literature in both dc and ac modes for the same family of SCO compounds. Indeed, from dc transport measurements above room temperature the values extracted were 340−520[36] and 417−1085 meV.[37] In the same conditions, ac transport measurements led to energy barriers of 500 and 200 meV at frequencies of 10 Hz and 1 MHz, respectively.[22] To explain these differences, one may consider that TRMC is sensitive to carrier motion within the particles, i.e., intraparticle movement, and that the incident penetration depth of the laser is in general on the order of 100 nm, that is, about the NP diameter studied here with TRMC.[38,39] In contrast, at megahertz frequencies the charge carriers are more likely forced to cross several grain boundaries while forcing the latter to flow through thicker powder samples, thus increasing the chances of interactions with impurities.[40,41]

The difference in energy barrier can thus be understood from the length scales probed in the experiments: the lower limit of the charge carrier diffusion x_{diff} inside the NPs occurring during one-half oscillating microwave cycle can be evaluated as[34]

DOI: 10.1021/acs.jpclett.8b02267
J. Phys. Chem. Lett. 2018, 9, 5672−5678

$$x_{\text{diff}} = \left(\frac{\sum \mu_{\text{min}} \cdot k_B \cdot T}{f \cdot e} \right)^{1/2} \quad (4)$$

where k_B is Boltzmann's constant, T is the temperature, f is the electric field frequency (9 GHz), and e is the charge of an electron. This expression is valid for low microwave electric field strengths[40] ($\leq$100 V cm^{-1}). The diffusional motion falls in a range of 2 nm at 100 K up to 5 nm at 360 K. It represents a local displacement of 1−3 or 3−7 repeat unit cells respectively along the interchain a and intrachain b axes of the crystal packing of $[Fe(Htrz)_2(trz)](BF_4)$.[28]

Further insight can be obtained by considering the half-life times, defined as the time needed for the TRMC signal to decay to half of its maximum. Importantly, half-life times significantly vary with temperature as shown in Figure 5 while,

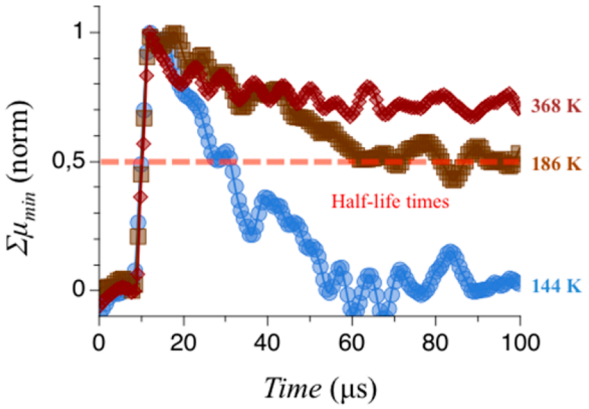

Figure 5. Normalized mobility decay dynamics versus time for different temperatures obtained after laser pulses exciting at 530 nm. Half-life times are plotted in Figure 6 for the whole temperature range.

as demonstrated in Figure S10 in the Supporting Information, the reference measurements showed no temperature dependence of the decay time kinetics of the TRMC signal. Figure 6 displays TRMC decay kinetics evaluated over the whole temperature range via a stretched exponential function up to

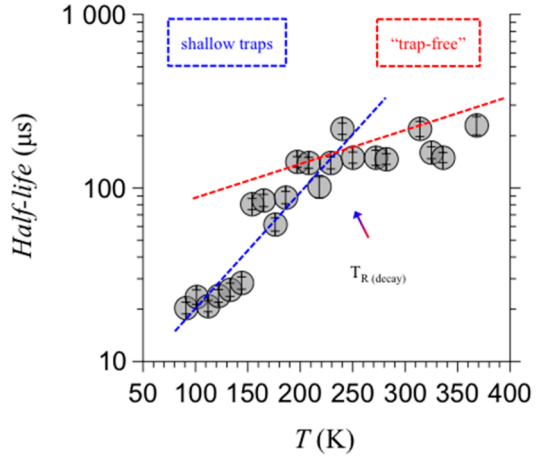

Figure 6. Half-life times, extracted from exponential fits of the TRMC signals shown in Figure 5, as a function of temperature. Measurements were obtained with a 530 nm pump fluence of 2.45 × 10^{15} photons per pulse. The dashed lines are drawn as a guide for the eyes.

the ms-range. Half-life times of ca. 200 μs take place at high temperature and decrease by 1 order of magnitude near liquid nitrogen temperature. These values are beyond the upper time window of the system of ca. 100 μs and suggest an efficient spatial separation of electrons and holes[35] especially at high temperatures. Besides, these TRMC signals follow two temperature-dependent exponential decays. The observed decrease of the half-life times with temperature is in contrast to the temperature dependence reported in organic solar cell compounds, where higher mobilities lead usually to faster decays.[42] Therefore, we stress that for these SCO compounds, the decay kinetics is not correlated to the charge carrier mobilities.

It is tempting to relate the two temperature-dependent regimes of the mobility and the decay kinetics of the charge carriers above-mentioned. Further experiments and theoretical calculations are needed to shed light on a closed relationship. In this scenario and at low temperatures, below T_R, the small activation energy of 3 meV associated with short lifetimes of the charge carriers suggests that transport is limited by shallow-trap states, away from a few k_BT from the HOMO levels of the SCO NPs.[43] In other words, the averaged trapping time of charge carriers at shallow traps remains much longer than the average time of diffusive motion between the trapping events, which explains the low mobilities and short lifetimes observed at low temperatures. Above T_R, these trapped states are thermally released, yielding a thermally activated hopping regime, where longer hops increase the mobility but, in counterpart, also the barrier energy. The activation energy could originate from inherent factors, such as molecular packing, dynamic disorder of the lattice (nonpolaronic in nature), polaronic self-localization, and competition between coherent and hopping motion of polarons.[44]

Efficient coupling of the charge carriers to the lattice vibrations of quasi-organic SCO compounds is expected and even more pronounced for those exhibiting a wide memory effect, as strong cooperative interactions via electron−phonon coupling between molecules changing spin states are required. For this reason, the observed thermally activated conductivity at higher temperatures in SCO compounds has been suggested to arise from a hopping polaron transport mechanism.[36] In other words, the charge carrier wave functions being localized on a few molecular units in our SCO compound could be of polaronic nature and would fall into different types of polaron formation depending on the electron hopping energy and the electron−phonon coupling,[45] which is specific for each SCO compound.

However, disorder is inevitably present in crystalline SCO compounds and could also contribute to the transport properties above T_R. In this context, diverse contributions of disorder should be considered: disorder has a time-dependent dynamic and/or a time-independent static origin. Dynamical disorder, present even for defectless ideal crystals, encompasses not only local polaronic carriers but also nonlocal lattice vibrations along and/or between interacting $[Fe(Htrz)_2(trz)]_n$ chains. It is important to realize that the small sizes of these NPs and the presence of the silica shell can also drastically modify the intrinsic phononic density of states of the NPs, as underlined recently.[46] However, static disorder of lattice vibrations may originate from both structural defects and impurities. For this SCO compound one can envision not only several types of chemical and physical defects especially in the vicinity of the SCO/silica interface such as 1D chain breaks,

DOI: 10.1021/acs.jpclett.8b02267
J. Phys. Chem. Lett. 2018, 9, 5672−5678

ring torsions of the triazoles leading to conformational torsions, bending and elongation of the 1D Fe^{II} chains but also a global loosening of the orthorhombic crystal packing.[47] Consequently, static disorder results in erratic inter- and/or intramolecular hopping integrals between sites causing variations of the kinetic energy of carrier hopping hindering high carrier mobilities as observed in this work.

It is important to mention that usually holes and electrons differ strongly in their sensitivity to be trapped at defects or impurities, or to interact with vibrational modes. However, the TRMC technique does not allow us to distinguish between holes and electrons in nature. In the search of a comprehensive examination of the transport properties of SCO nanomaterials, a complementary direct-current method such as time-of-flight (TOF) combined to TRMC measurements could unveil the genuine nature of the charge carrier and give an estimation of the optical quantum yield (ϕ). In further experiments the temperature and electric field dependence offered by the use of a TOF technique should shed light on the origin of the charge carrier-trapping mechanism (polarons and/or disorder).

Besides, the use of a color insensitive method such as electron pulse-radiolysis TRMC[48] might allow us to compare the intrinsic mobilities of charge carriers in both spin states. This work is in progress.

As nonspherical (SCO) objects can be manipulated to align their major axis in the direction of the electrical field,[16] we envision that tuning the polarization of a gigahertz−terahertz beam in-plane and out-of-plane could bring unassessed anisotropy transport (i.e., comparison between intra and inter Fe(II) chain transport), which remains a fundamental question to tackle.

In conclusion, we have presented a contactless time-resolved microwave conductivity (TRMC) study on spin-crossover (SCO) compounds that offers an alternative to dielectric techniques and dc/ac electrical measurements performed between electrodes. Thanks to its gigahertz dynamics microwave probe, TRMC probes nanoscale charge transport of mobile photogenerated charge carriers in ∼100 nm size hybrid SCO@SiO_2 NPs of $[Fe(Htrz)_2(trz)](BF_4)$. We have determined a lower limit of the local charge carrier mobility in the LS state, ranging from 5×10^{-6} up to 9×10^{-6} cm^2 V^{-1} s^{-1}, respectively, from room temperature up to 360 K. TRMC measurements from 77 K up to 360 K have shown two well-defined regimes in the mobility and the half-life times, which possess similar transition temperatures. We propose that these two transport regimes in the LS state can be rationalized in terms of a transition where charge carriers are tunnelling between shallow traps, toward a trap-free hopping regime thermally activated at higher temperatures where longer hops increase the mobility but at the same time also the barrier energy.

■ ASSOCIATED CONTENT

Supporting Information

The Supporting Information is available free of charge on the ACS Publications website at DOI: 10.1021/acs.jpclett.8b02267.

Experimental and characterization details, size distribution graph, TEM image, dark field STEM images, EDS map images, absorbance and diffuse reflectance spectra, laser light transmittance graph, schematic of the time-resolved microwave photoconductance setup, graphs of conductance change vs time and temperature, 2D-TRMC signals, (PDF)

Thermochromic effect above room temperature from purple to white/yellow in a powder sample of SCO@SiO_2 NPs (MOV)

■ AUTHOR INFORMATION

Corresponding Authors

*J.D. E-mail: Julien.dugay@gmail.com.

*E.C. E-mail: eugenio.coronado@uv.es.

ORCID

Julien Dugay: 0000-0002-4384-1315

Mónica Giménez-Marqués: 0000-0002-4931-5711

Notes

The authors declare no competing financial interest.

■ ACKNOWLEDGMENTS

The present work has been funded by the EU (COST Action CA15128 MOLSPIN and project COSMICS, 766726), the Spanish MINECO (Unit of excellence "María de Maeztu" MDM-2015-0538 and project MAT2017-89993-R), and the Generalitat Valenciana (Prometeo Program of excellence). M.G.-M. thanks Spanish MICINN for a Juan de la Cierva-Incorporation grant. We thank Prof. Dr. Laurens Siebbeles and Dr. ir. T. J. Savenije for fruitful discussions.

■ REFERENCES

(1) (a) Gütlich, P.; Goodwin, H. A. In *Spin Crossover Transit. Met. Compd. I*; Springer: Berlin, Heidelberg, 2004; pp 1−47. (b) Gütlich, P.; Goodwin, H. A.; Létard, J.-F.; Guionneau, P.; Goux-Capes, L. In *Spin Crossover Transit. Met. Compd. III*; Springer: Berlin, Heidelberg, 2004; pp 1−19.

(2) Murray, K. S.; Kepert, C. J. In *Spin Crossover Transit. Met. Compd. I*; Gütlich, P., Goodwin, H. A., Eds.; Springer: Berlin, Heidelberg, 2004; pp 195−228.

(3) Real, J. A.; Gaspar, A. B.; Muñoz, M. C. *Dalton Trans* **2005**, *2062*, 2062.

(4) Gamez, P.; Costa, J. S.; Quesada, M.; Aromí, G. *Dalton Trans.* **2009**, *7845*, 7845.

(5) Jureschi, C.-M.; Linares, J.; Boulmaali, A.; Dahoo, P. R.; Rotaru, A.; Garcia, Y. *Sensors* **2016**, *16*, 187.

(6) Giménez-Marqués, M.; de Larrea, M. L . G.-S.; Coronado, E. *J. Mater. Chem. C* **2015**, *3*, 7946.

(7) Freysz, E.; Montant, S.; Létard, S.; Létard, J.-F. *Chem. Phys. Lett.* **2004**, *394*, 318.

(8) Gallé, G.; Etrillard, C.; Degert, J.; Guillaume, F.; Létard, J.-F.; Freysz, E. *Appl. Phys. Lett.* **2013**, *102*, 063302.

(9) Rotaru, A.; Gural'skiy, I. A.; Molnár, G.; Salmon, L.; Demont, P.; Bousseksou, A. *Chem. Commun.* **2012**, *48*, 4163.

(10) Lefter, C.; Tricard, S.; Peng, H.; Molnár, G.; Salmon, L.; Demont, P.; Rotaru, A.; Bousseksou, A. *J. Phys. Chem. C* **2015**, *119*, 8522.

(11) Lefter, C.; Gural'skiy, I. A.; Peng, H.; Molnár, G.; Salmon, L.; Rotaru, A.; Bousseksou, A.; Demont, P. *Phys. Status Solidi RRL* **2014**, *8*, 191.

(12) Rotaru, A.; Dugay, J.; Tan, R. P.; Guralskiy, I. A.; Salmon, L.; Demont, P.; Carrey, J.; Molnár, G.; Respaud, M.; Bousseksou, A. *Adv. Mater.* **2013**, *25*, 1745.

(13) Lefter, C.; Tan, R.; Dugay, J.; Tricard, S.; Molnár, G.; Salmon, L.; Carrey, J.; Rotaru, A.; Bousseksou, A. *Phys. Chem. Chem. Phys.* **2015**, *17*, 5151.

(14) Lefter, C.; Tan, R.; Tricard, S.; Dugay, J.; Molnár, G.; Salmon, L.; Carrey, J.; Rotaru, A.; Bousseksou, A. *Polyhedron* **2015**, *102*, 434.

DOI: 10.1021/acs.jpclett.8b02267
J. Phys. Chem. Lett. 2018, 9, 5672−5678

(15) Lefter, C.; Tan, R.; Dugay, J.; Tricard, S.; Molnár, G.; Salmon, L.; Carrey, J.; Nicolazzi, W.; Rotaru, A.; Bousseksou, A. *Chem. Phys. Lett.* **2016**, *644*, 138.
(16) Rotaru, A.; Dugay, J.; Tan, R. P.; Guralskiy, I. A.; Salmon, L.; Demont, P.; Carrey, J.; Molnár, G.; Respaud, M.; Bousseksou, A. *Adv. Mater.* **2013**, *25*, 1745.
(17) Dugay, J.; Giménez-Marqués, M.; Kozlova, T.; Zandbergen, H. W.; Coronado, E.; van der Zant, H. S. J. *Adv. Mater.* **2015**, *27*, 1288.
(18) Holovchenko, A.; Dugay, J.; Giménez-Marqués, M.; Torres-Cavanillas, R.; Coronado, E.; van der Zant, H. S. J. *Adv. Mater.* **2016**, *28*, 7228.
(19) Prins, F.; Monrabal-Capilla, M.; Osorio, E. A.; Coronado, E.; van der Zant, H. S. J. *Adv. Mater.* **2011**, *23*, 1545.
(20) Rotaru, A.; Dugay, J.; Tan, R. P.; Guralskiy, I. A.; Salmon, L.; Demont, P.; Carrey, J.; Molnár, G.; Respaud, M.; Bousseksou, A. *Adv. Mater.* **2013**, *25*, 1745.
(21) Lefter, C.; Tan, R.; Dugay, J.; Tricard, S.; Molnár, G.; Salmon, L.; Carrey, J.; Rotaru, A.; Bousseksou, A. *Phys. Chem. Chem. Phys.* **2015**, *17*, 5151.
(22) Lefter, C.; Tricard, S.; Peng, H.; Molnár, G.; Salmon, L.; Demont, P.; Rotaru, A.; Bousseksou, A. *J. Phys. Chem. C* **2015**, *119*, 8522.
(23) Kroeze, J. E.; Savenije, T. J.; Vermeulen, M. J. W.; Warman, J. M. *J. Phys. Chem. B* **2003**, *107*, 7696.
(24) Savenije, T. J.; Ferguson, A. J.; Kopidakis, N.; Rumbles, G. *J. Phys. Chem. C* **2013**, *117*, 24085.
(25) Haasnoot, J. G.; Vos, G.; Groeneveld, W. L. *Z. Naturforsch., B: J. Chem. Sci.* **1977**, *32*, 1421.
(26) Kahn, O.; Kröber, J.; Jay, C. *Adv. Mater.* **1992**, *4*, 718.
(27) Urakawa, A.; Van Beek, W.; Monrabal-Capilla, M.; Galán-Mascarós, J. R.; Palin, L.; Milanesio, M. *J. Phys. Chem. C* **2011**, *115*, 1323.
(28) Grosjean, A.; Négrier, P.; Bordet, P.; Etrillard, C.; Mondieig, D.; Pechev, S.; Lebraud, E.; Létard, J.-F.; Guionneau, P. *Eur. J. Inorg. Chem.* **2013**, *2013*, 796.
(29) Titos-Padilla, S.; Herrera, J. M.; Chen, X.-W.; Delgado, J. J.; Colacio, E. *Angew. Chem.* **2011**, *123*, 3348.
(30) Ponseca, C. S.; Hutter, E. M.; Piatkowski, P.; Cohen, B.; Pascher, T.; Douhal, A.; Yartsev, A.; Sundström, V.; Savenije, T. J. *J. Am. Chem. Soc.* **2015**, *137*, 16043.
(31) Sandeep, C. S. S.; ten Cate, S.; Schins, J. M.; Savenije, T. J.; Liu, Y.; Law, M.; Kinge, S.; Houtepen, A. J.; Siebbeles, L. D. A. *Nat. Commun.* **2013**, *4*, 2360.
(32) Savenije, T. J.; Kroeze, J. E.; Yang, X.; Loos, J. *Adv. Funct. Mater.* **2005**, *15*, 1260.
(33) Shi, S.; Schmerber, G.; Arabski, J.; Beaufrand, J.-B.; Kim, D. J.; Boukari, S.; Bowen, M.; Kemp, N. T.; Viart, N.; Rogez, G.; Beaurepaire, E.; Aubriet, H.; Petersen, J.; Becker, C.; Ruch, D. *Appl. Phys. Lett.* **2009**, *95*, 043303.
(34) Bird, M. J.; Reid, O. G.; Cook, A. R.; Asaoka, S.; Shibano, Y.; Imahori, H.; Rumbles, G.; Miller, J. R. *J. Phys. Chem. C* **2014**, *118*, 6100.
(35) Tokarev, A.; Salmon, L.; Guari, Y.; Nicolazzi, W.; Molnár, G.; Bousseksou, A. *Chem. Commun.* **2010**, *46*, 8011.
(36) Rotaru, A.; Gural'skiy, I. A.; Molnar, G.; Salmon, L.; Demont, P.; Bousseksou, A. *Chem. Commun.* **2012**, *48*, 4163.
(37) Holovchenko, A.; Dugay, J.; Giménez-Marqués, M.; Coronado, E.; van der Zant, H. S. J. *ArXiv160204681 Cond-Mat* **2016**.
(38) Grozema, F. C.; Siebbeles, L. D. A. *J. Phys. Chem. Lett.* **2011**, *2*, 2951.
(39) Ferguson, A. J.; Kopidakis, N.; Shaheen, S. E.; Rumbles, G. *J. Phys. Chem. C* **2011**, *115*, 23134.
(40) Dicker, G.; de Haas, M. P.; Siebbeles, L. D. A.; Warman, J. M. *Phys. Rev. B: Condens. Matter Mater. Phys.* **2004**, *70*, 045203.
(41) Katoh, R.; Huijser, A.; Hara, K.; Savenije, T. J.; Siebbeles, L. D. A. *J. Phys. Chem. C* **2007**, *111*, 10741.
(42) Savenije, T. J.; Murthy, D. H. K.; Gunz, M.; Gorenflot, J.; Siebbeles, L. D. A.; Dyakonov, V.; Deibel, C. *J. Phys. Chem. Lett.* **2011**, *2*, 1368.
(43) Sakanoue, T.; Sirringhaus, H. *Nat. Mater.* **2010**, *9*, 736.
(44) Pingel, P.; Zen, A.; Abellón, R. D.; Grozema, F. C.; Siebbeles, L. D. A.; Neher, D. *Adv. Funct. Mater.* **2010**, *20*, 2286.
(45) Barišić, O. S.; Barišić, S. *Eur. Phys. J. B* **2008**, *64*, 1.
(46) Félix, G.; Mikolasek, M.; Peng, H.; Nicolazzi, W.; Molnár, G.; Chumakov, A. I.; Salmon, L.; Bousseksou, A. *Phys. Rev. B: Condens. Matter Mater. Phys.* **2015**, *91*, 024422.
(47) Tummala, N. R.; Zheng, Z.; Aziz, S. G.; Coropceanu, V.; Brédas, J.-L. *J. Phys. Chem. Lett.* **2015**, *6*, 3657.
(48) Warman, J. M.; de Haas, M. P.; Dicker, G.; Grozema, F. C.; Piris, J.; Debije, M. G. *Chem. Mater.* **2004**, *16*, 4600.

DOI: 10.1021/acs.jpclett.8b02267
J. Phys. Chem. Lett. 2018, 9, 5672−5678